CERN-THESIS-2016-400
/ /2016

**ENS 491-492**

# Development of Single Sideband Down Converters for Precise Measurements of the Axial Frequency of a Single Trapped Antiproton

**Bachelor Thesis**

Mustafa Beşirli

Supervised by Yaşar Gürbüz and Stefan Ulmer

May, 14 2016

---

Faculty of Engineering and Natural Sciences

Sabanci University

Electronics Engineering

---

# Abstract

The Baryon Antibaryon Symmetry Experiment (BASE) at the antiproton decelerator of CERN, Geneva, Switzerland aims at precise comparisons of the fundamental properties of the antiproton and proton. Such comparisons are interesting because any measured asymmetry between a matter and antimatter-conjugates would hint at physics beyond the Standard Model. In this experiment, a single antiproton is prepared in a cryogenic Penning trap, and all information about this trapped particle is obtained by detecting image currents in the trap electrodes, which are induced by the motion of the trapped charged particle. The detected image currents are in the fA range, which requires the use of ultra-low noise electronics. Axial signals of the proton or antiproton are analyzed with Fast Fourier transform (FFT) analyzers to meet high frequency resolution. The axial frequency is at about 680 kHz in the so-called analysis trap of our apparatus. However, the upper frequency limit of the available FFT analyzers which meet the required frequency resolution is at around 100 kHz. Therefore, signals containing frequencies higher than the maximum frequency should be converted down into the frequency range of the analyzer to become measurable.

In this graduation project, a single sideband (SSB) down converter for the measurement of the axial frequency of an antiproton or a proton is developed. The goal is to down-convert the axial frequency into the frequency range of the FFT analyzer and to increase the down-mixed signal to noise ratio of the detection system. In addition we developed an active feedback cooling system by using this SSB down converter. The temperature of the axial detection system is about 8 Kelvin without feedback. It is demonstrated that the feedback system is capable to decrease the temperature of the detection system and thus that of the particle by about a factor of 3 to 5. This leads to reduction of resonance line widths, faster particle preparation cycles and thus improves measurement precision.

In this thesis, the principle of the experiment, and the development of a SSB down converter and active feedback cooling system are described.

# Table of Contents

# List of Figures

# Chapter 1

# Introduction

The axial frequency signals of an antiproton or a proton are measured with FFT analyzers when both a high frequency resolution and a high dynamic range are required. The BASE Collaboration uses SR780 Dynamic Signal Analyzers from Stanford Research Systems with a bandwidth from DC to 102.4 kHz. We developed an SSB down converter to down-convert signals containing frequencies higher than the maximum frequency of the analyzer into the frequency range accepted by the FFT analyzer. After that, we developed an active feedback cooling to decrease the temperature of the axial detector from 8 Kelvin to around 1.8 Kelvin. So, we can compare the fundamental properties of an antiproton and a proton more precisely.

Firstly, we can explain the working principle of SSB down converter. In simple down conversion method, the complete frequency range of interest is either in the upper sideband, i.e. above the LO oscillator frequency $\nu_{LO}$, or in the lower sideband, i.e. below $\nu_{LO}$. A single multiplier followed by a low-pass filter converts both signals from the upper and the lower sideband down into the same frequency range. Signals at lower sideband and upper sideband are converted to same intermediate frequency *IF* and these signals are added. That means noise is added to the signal from the frequency range of interest and signal to noise ratio (SNR) is reduced. Therefore, we aim to reject unwanted sideband to increase the SNR of detection systems. The system which rejects unwanted sideband is called as single sideband down conversion. If the unwanted sideband is rejected, the signal to noise ratio will be enhanced in a factor of 2. So, the limit of SNR improvement is 3dB. The working principle of single sideband down converter is shown in Figure 1.1. Two mixers, two low pass filters, two phase shifters and a differential amplifier will be used to implement a SSB down converter.

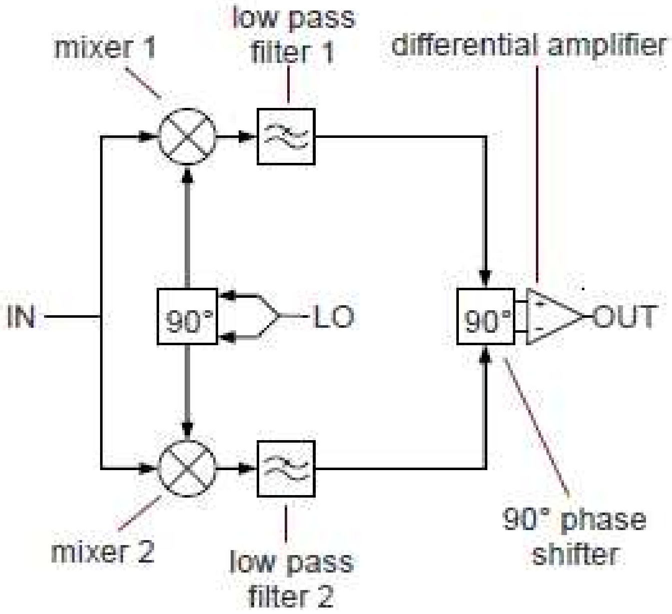


Figure 1.1: SSB down converter design

At first, we can consider the signal from the upper sideband. The signal is applied to the mixers in the setup. The two local oscillator signals of the mixers have equal frequency $\nu_{LO}$ and equal amplitude, but the local oscillator signal for mixer 1 is 90° ahead in phase. Then, the signals are filtered by low pass filters and both signals are converted to same frequency *IF* and both signals have same amplitude. However, signal behind the mixer 2 is 90° ahead in phase. Then the second phase shifter increases the phase difference between the signal behind mixer 1 and the signal behind signal 2 by another 90°, so that the signal behind mixer 2 is 180° ahead in phase. So, the differential amplifier superimposes the two signals constructively. Secondly, we can consider the signal from the lower sideband. The signal is again applied to the both mixers and the properties of local oscillator signals are same as in the case of upper sideband. After low pass filter, the signals are both at frequency *IF* and of equal amplitude. In contrast, signal behind mixer 1 is 90° ahead in phase in this case. Therefore, the second phase shifter changes the phase difference between the signal behind the mixer 1 and the signal behind the mixer 2 to 0°. So, the differential amplifier superimposes the two signals destructively [1]. As a result, the unwanted sideband is rejected and we expect to gain 3dB increase in SNR.

After that, we developed an active feedback cooling system by using this SSB converter. We implemented this circuitry to the output of the axial detector and we aim to decrease the detector temperature in a factor of three to five. So, we can have reduced line width in the FFT analyzer and make more accurate measurements.

In addition, I have also developed cryogenic filters for the spin-flip lines. Strong drives are needed to drive spin transition, and this creates noise in the frequency spectrum of the cyclotron frequency and also magnetron frequency. We aim to block this noise effect by applying these filters. Details will be explained Chapter 6.

# Chapter 2

# Project Proposal

The Baryon Antibaryon Symmetry Experiment (BASE) aims at a stringent test of the combined charge parity and time reversal (CPT) symmetry by comparing the magnetic moments and charge-to-mass ratios of the proton and the antiproton with high precision [2,3]. According to CPT symmetry, the fundamental properties of matter and antimatter-conjugates are predicted to be identical [4]. For instance, the magnetic moments of the antiproton and the proton have opposite signs, but are at exactly the same value. Using single particles in a Penning trap, the proton /antiproton g-factors, i.e. the magnetic moment in units of nuclear magneton, are determined by measuring the respective ratio of the spin-procession frequency (Larmor frequency) to the cyclotron frequency [5].

The Larmor frequency is measured by application of the elegant continuous Stern-Gerlach effect [6]. A magnetic bottle which is superimposed on the trap leads to a change of the axial frequency caused by a spin flip. By detecting these changes as a function of variable radio-frequencies which induce the spin transitions, the spin flip probability as a function of the drive frequency is recorded [5,6]. This enables the measurement of the antiproton's Larmor frequency. The axial frequency change caused by a spin-flip is at about 180 mHz out of 680kHz [2]. In order to resolve such tiny axial frequency changes, high resolution in the axial frequency measurements is required. Therefore, we apply active feedback cooling to decrease the temperature of the detection system. As a result, line widths in B-field are reduced and it results in a reduction in line width of the Larmor resonance as shown in Figure 2.1. So, the Larmor frequency can be measured more precisely. In addition, if the axial temperature is decreased, the magnetron temperature will also be reduced and sideband cooling will be much faster.

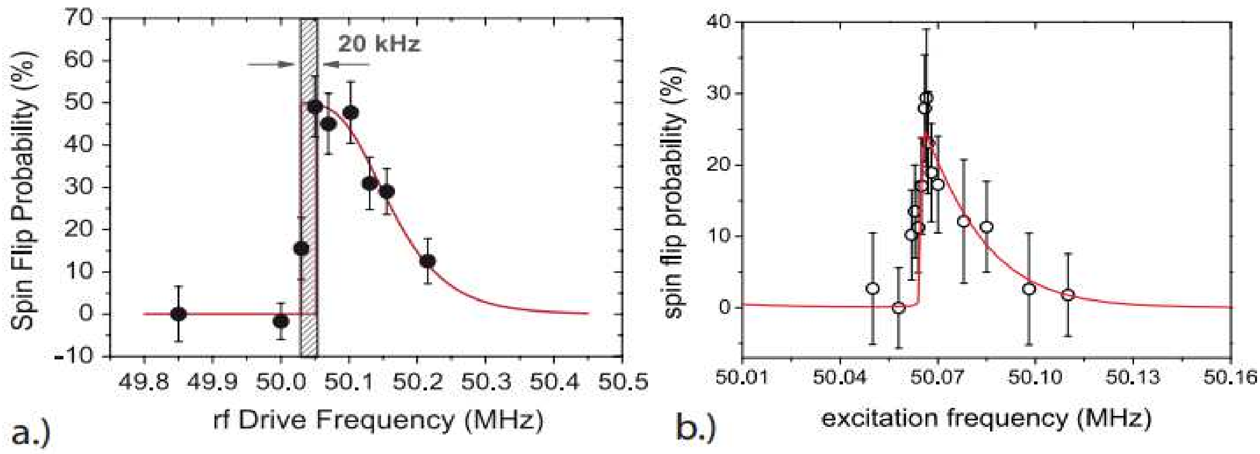


Figure 2.1: Larmor resonance without feedback (left) and with feedback (right)

Without the feedback cooling system, the low-noise amplifier stage (LNA) at 300 Kelvin stage is connected to the FFT analyzer via a down converting mixer. In the active feedback cooling as shown in Figure 2.2, the output of the LNA is connected to the single sideband (SSB) down converter. After that, the signal from the SSB down converter goes to a power splitter. Half of the power of the signal is connected to the FFT analyzer to observe the noise spectrum of the detector, and the other half is connected to the axial detector via an up converter, a band pass filter and a voltage controlled attenuator (VCA). The output of the VCA is connected to the detection system via a loosely coupled capacitance. For this project, I developed a single sideband (SSB) down converter, an up converter, band pass filter and a voltage controlled attenuator.

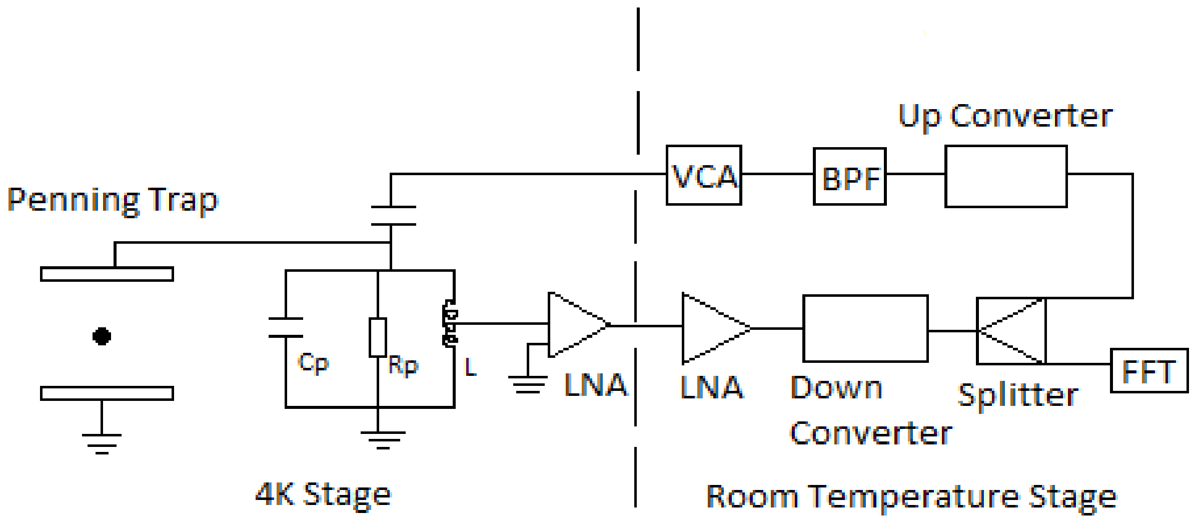


Figure 2.2: Schematic of active feedback cooling system consists of an SSB down converter, a power splitter, an up converter, a BPF and a VCA. For further discussions see Chapter 5.

The temperature of the axial detection system is around 8 Kelvin. By using the active feedback cooling, we intend to decrease this temperature by a factor of three to five [7]. By decreasing the temperature, lower drive power are required to drive the spin resonances. In measurements reduced line widths will be observed and the time required for preparation procedures to cool the radial modes will decrease. In total these advances will lead to more accurate frequency measurements at reduced systematic effects.

# Chapter 3

# Measurement of the proton–antiproton g-factor

Aiming at measuring the proton-antiproton g-factor with ultra-high precision, the BASE collaboration uses cryogenic Penning traps. In the first part of this chapter, the behavior of a single particle stored in such a trap is presented. Afterwards, the ultra-sensitive superconducting detection systems of the BASE apparatus will be described. Lastly, the g-factor measurement will be explained briefly.

### 3.1 Particle Motion in a Penning Trap

The BASE Collaboration uses cryogenic Penning traps in order to measure the antiproton g-factor with ultra-high precision. In a magnetic field B, a particle of mass *m* and charge *q* is constrained to a circular orbit. This is the so-called "free-cyclotron motion". Its frequency is given by:

$$\omega_c = \frac{|q\boldsymbol{B}|}{m}.$$

The cyclotron motion is a radial motion, thus it is bound radially but not axially. In a Penning trap, an electrostatic quadrupole potential is superimposed to confine the particle also in the axial direction. The electric and magnetic field configuration of a Penning trap is shown in Figure 3.1.

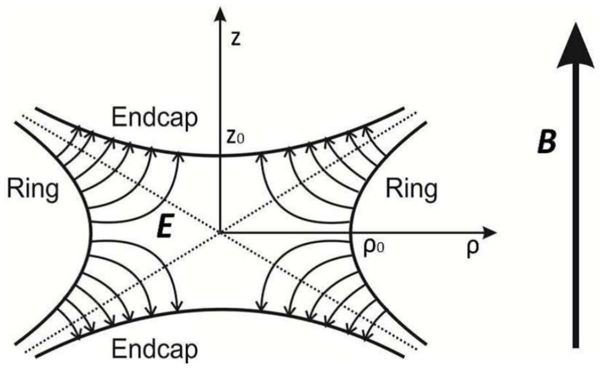


Figure 3.1: Electric and magnetic field configuration of a Penning trap

The magnetic field confines the particle only in radial direction. Together with the electrostatic quadrupole potential, the particle is confined also in the axial direction. In order to generate the quadrupole potential, three electrodes are required. There are two endcap electrodes on the top and the bottom, and one ring electrode in the center [2,8].

The charged particle is stored with an axial frequency of:

$$\omega_z = \sqrt{\frac{2qC_2V_0}{m}}$$

The radial field component of the electrostatic quadrupole potential leads to a modification of the free cyclotron motion. The resulting eigen-frequency of this modified cyclotron motion is

$$\omega_+ = \frac{1}{2}(\omega_c + \sqrt{\omega_c^2 - 2\omega_z^2})$$

In addition, the so-called “magnetron motion” occurs, which is the second radial eigenmotion caused by a drift in the crossed ***E x B*** field of the trap. The magnetron frequency is

$$\omega_- = \frac{1}{2}(\omega_c - \sqrt{\omega_c^2 - 2\omega_z^2}) .$$

To sum up, the particle moves in a Penning trap in three independent eigenmotions [6,9]. These are the axial motion 680 kHz, the magnetron motion at 7kHz and the modified cyclotron motion, in our case at 29.656 MHz [2]. In Figure 3.2 a.), a section-view of a cylindrical Penning trap and the three eigenmotions (3.2.b.)) are shown.

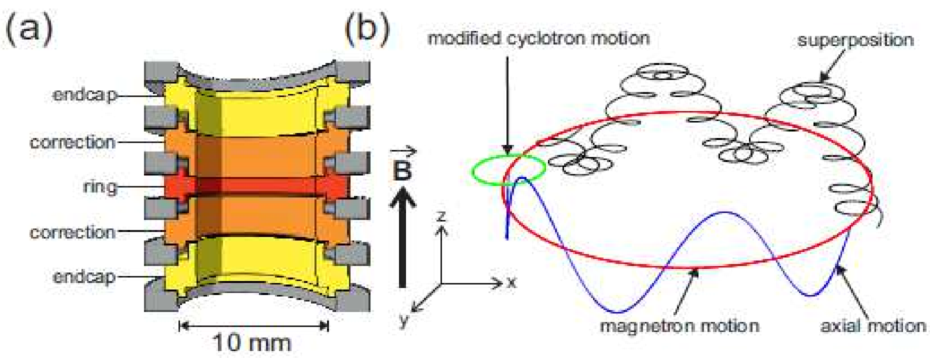


Figure 3.2: (a) Cut view of cylindrical Penning trap, (b) The composition of the motion of a particle inside Penning trap

### 3.2 Detection Systems

Information on the three eigenmotions in a Penning trap can be extracted by the detection of image currents, which are induced in the trap electrodes caused by the oscillating particle [6,9]. Figure 3.3 illustrates the image current detection principle in a Penning Trap.

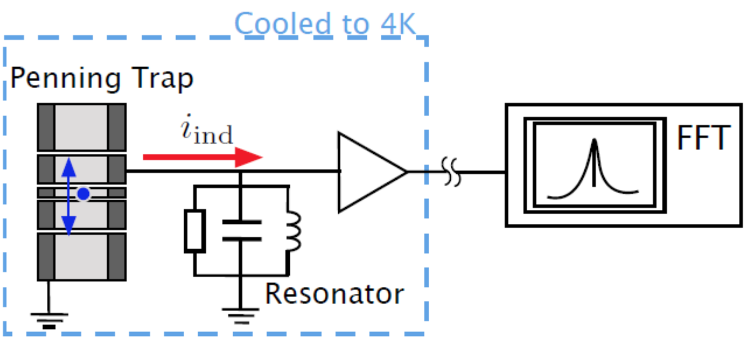


Figure 3.3: Illustration of the image current detection principle in a Penning trap

In a Penning trap eigenmotions of a particle induces tiny image current in the electrodes, and a high Q-value resonator and an ultra-low noise amplifier are connected to one of the Penning trap electrodes [10, 11]. These image current is converted to a voltage drop using a resonant tuned circuit as shown in Figure 3.4(a). A particle in thermal equilibrium with the detection system can be represented by an equivalent series tuned circuits, which shunts the thermal noise of the detection system at the motional frequency of the particle (3.4.(b)).

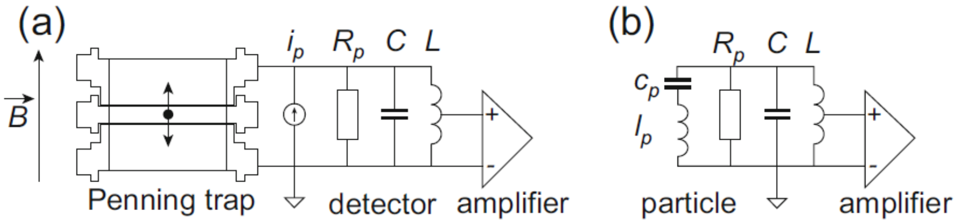


Figure 3.4: (a) Schematic of a Penning Trap and the detection system (b) A particle in thermal equilibrium with detection system can be represented by an equivalent series tuned circuit

Consequently it shorts the thermal noise of the detection system, and appears as a dip in the detector's noise resonance [10]. Figure 3.5(a) shows of an axially excited single trapped antiproton turned to resonance an axial detector. The appearance of the particle dip is shown in Figure 3.5(b) [12].

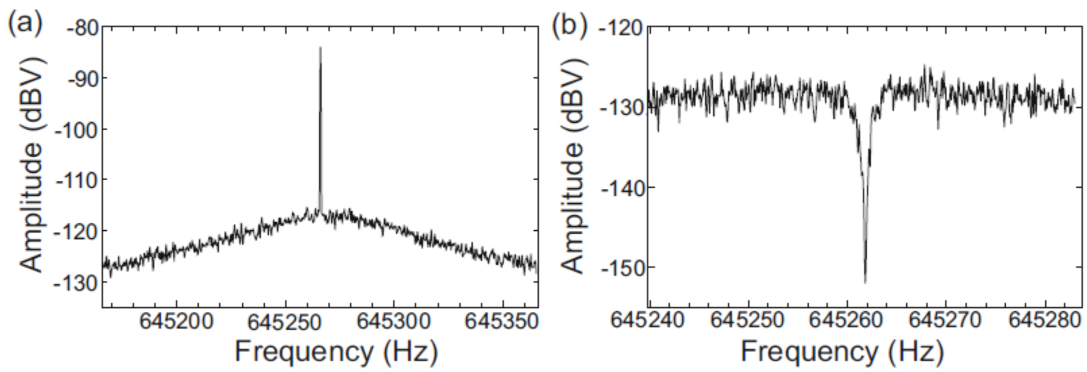


Figure 3.5: (a) FFT signal of an axially excited single trapped antiproton (b) Particle shunts the thermal noise of the detector at its eigen-frequency and appears as a dip.

As a large signal to noise ratio (SNR) reduces the frequency scatter, the major goal is to increase SNR. In case of a dip detection, SNR is defined by the ratio of the Johnson-Nyquist noise of the tank circuit $u_n$ [nV / √Hz] to an equivalent input noise of the amplifier $e_n$ [13] [14]:

$$u_n = \sqrt{4k_B T R_{eff}} \cdot \kappa$$

$$\text{SNR} = \frac{u_n}{e_n} = \frac{\sqrt{4k_B T R_{eff}} \cdot \kappa}{e_n},$$

where $k_B$ is the Boltzmann constant, $T$ the temperature of the detector, $\kappa$ the coupling constant, and $e_n$ the equivalent input noise of the amplifier, respectively.

On resonance, the circuit in Figure 3.4(a) acts as a parallel resistance $R_p$:

$$R_p = 2\pi \nu_r Q L$$

where $\nu_r$ is the resonance frequency, $Q$ the quality factor of the resonator and $L$ the inductance value, respectively. By using large impedance, tiny image current signal is converted to a detectable voltage. Therefore, the $Q$-factor should be as large as possible to have a very sensitive detection system [15,16].

### 3.3 The g-factor measurement

The g-factor is a dimensionless quantity which relates the spin $\vec{S}$ of a particle to its magnetic moment

$$\vec{\mu_s} = g\frac{q}{2m}\vec{S},$$

where $q$ is the charge, and $m$ the mass of a particle, respectively. The energy of the spin precession in the magnetic field is called the Larmor precession with its frequency:

$$\omega_L = g\frac{q}{2m}B_z.$$

Together with the equation of the free cyclotron frequency, the g-factor can be expressed as the ratio of the Larmor frequency $\omega_L$ and the free cyclotron frequency $\omega_C$ [17,18,19]:

$$\omega_L = g \cdot \frac{\omega_c}{2} \iff g = 2\frac{\omega_L}{\omega_c}.$$

The cyclotron frequency of the trapped charged particle is related to the three independent eigenmotions via the invariance theorem [20]:

$$\nu_c^2 = \nu_+^2 + \nu_-^2 + \nu_z^2$$

Footnote 1: Quantities $\omega$ are related to frequencies ν as $\omega=2\pi\nu$. Within the test we switch between the two nomenclatures.

The Larmor frequency is measured by detecting the axial frequency change caused by spin flips [21]. The axial frequency change is about 180 mHz out of 680kHz. Figure 3.6 shows the change on the axial frequency due to the spin flips.

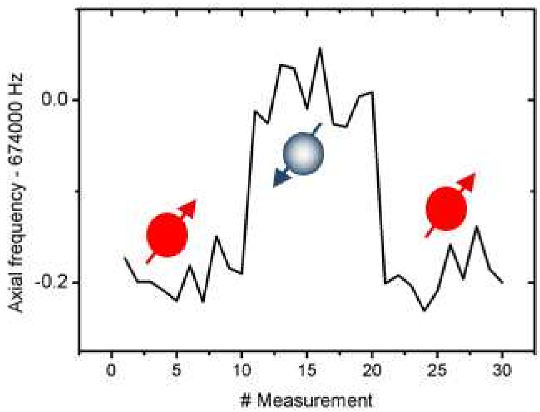


Figure 3.6: Larmor frequency measurement. The axial frequency change is about 180 mHz out of 680 kHz in case of spin transition.

In order to resolve such a tiny axial frequency change, we need to have a good resolution on the axial frequency. Therefore I developed SSB down converter and active feedback cooling system to decrease the temperature and to increase the SNR of the detector.

# Chapter 4

# Axial Frequency Down Converters

In this section, the theoretical concepts of down conversion, single sideband down conversion and design and implementation of such systems, and measurement results will be explained respectively.

### 4.1 Theoretical Concepts of Down Conversion

Down conversion is a multiplication process to convert a signal with high frequency to a lower desired frequency. In our case, we use SR780 Dynamic Signal Analyzer to measure the axial frequencies at 680kHz of the proton and the antiproton in both high frequency resolution and high dynamic range. The upper frequency limit of such analyzers are of order 100kHz, thus signals containing frequencies higher than upper frequency limit should be converted down into the frequency range of the analyzer to be detectable.

A down converter shifts the frequency $\nu_{in}$ of a signal to the so-called intermediate frequency $IF = \nu_{in} - \nu_{LO}$ by multiplying the signal with a local oscillator (LO) signal of frequency $\nu_{LO}$:

$$U_{out}(t) \propto \sin(2\pi \cdot \nu_{in} t) \cdot \sin(2\pi \cdot \nu_{LO} t)$$
$$= \frac{1}{2}(\sin(2\pi \cdot (\nu_{in} - \nu_{LO})t) + \sin(2\pi \cdot (\nu_{in} + \nu_{LO})t).$$

Afrer this multiplication, we have signals at the difference frequency and also at the sum frequency. For down conversion, the signal at the sum frequency has to be removed by a low pass filter. After the sum frequency the signal is filtered, and the down converted signal can be obtained. A single mixer and a LO signal is sufficient for a simple down conversion.

### 4.2 Single Sideband Down Converters

In a simple down conversion method, the complete frequency range of interest is either in the upper sideband, i.e. above the LO oscillator frequency $\nu_{LO}$, or in the lower sideband, i.e. below $\nu_{LO}$. A single multiplier followed by a low-pass filter converts both signals from the upper and the lower sideband down into the same frequency range. Signals at lower sideband and upper sideband are converted to same intermediate frequency *IF* and these signals are added. That means noise is added to the signal from the lower frequency sideband and the signal to noise ratio (SNR) of the superconducting axial detector is reduced. Therefore, we aim to reject the unwanted sideband to increase the SNR of detection systems after the conversion. System which reject unwanted sidebands are called single sideband down converters [1]. If the unwanted sideband is rejected, the signal to noise ratio will be enhanced by a factor of 2. So, the limit of the SNR improvement is 3dB. The working principle of a single sideband down converter is shown in Figure 4.1.

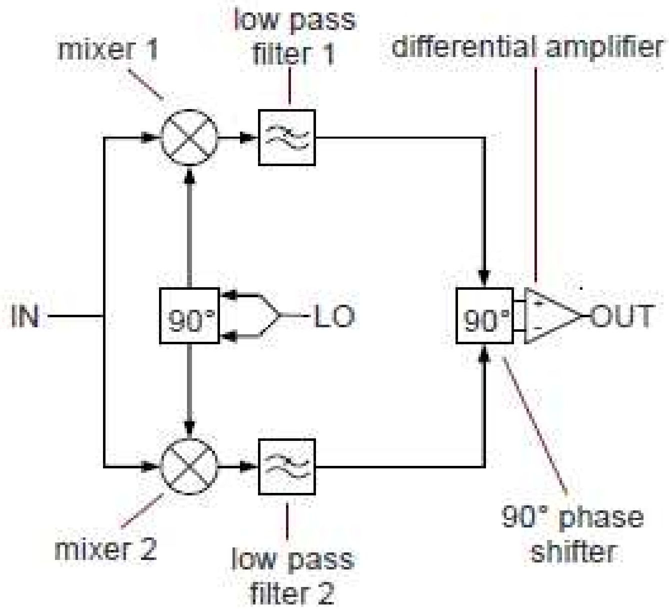


Figure 4.1: SSB down converter consists of 2 mixers, 2 LPFs, 2 phase shifters and a differential amplifier. For details see text.

An SSB down converter consists of 2 mixers, 2 low pass filters, two phase shifters and a differential amplifier. At the output of the phase shifters, two signals at *IF* are created and these signals are constructively superimposed for input signals from one sideband and destructively for the other sideband.

In our case, we aim to measure the axial motion of a single antiproton. The axial frequency of a single antiproton in our apparatus is about 680 kHz. Therefore, the axial signal should be converted down into the frequency range of the analyzer. So, we decided to convert it down to 50 kHz. The input signal at frequency $\nu_{LO} + IF$ should be converted to an intermediate frequency $IF$. However, the signal at the image frequency is also converter down to $IF$.

$$\nu_{IN} = \nu_{LO} + IF$$

$$\nu_{IN} = \nu_{LO} - IF$$

For instance, the axial signal at 680 kHz should be converted down to 50 kHz. Therefore, the local oscillator frequency has to be 630 kHz, but the input signal at 580 kHz will be converted also to 50 kHz. Therefore, it will decrease the SNR by a factor of 2 being equivalent to a 3dB reduction. Therefore, we apply single sideband down conversion to eliminate the image frequency. The local oscillator frequency $\nu_{LO}$ has to be chosen such that the signal of interest is in the upper sideband. The signal from the lower sideband at frequency $\nu_{LO} - IF$ should be rejected in order not to disturb the measurement of the upper sideband signal.

We aim to convert the axial signal at 680 kHz down to 50 kHz. The local oscillator signals of the mixers are at equal frequency $\nu_{LO}$ at 630 kHz. The input signal which is at 680 kHz is from the upper sideband and mirror image signal which is at 580 kHz is from the lower sideband. Firstly, the signal from the upper sideband is considered. The signal is applied to the two mixers in the setup. The local oscillator signals of equal frequency $\nu_{LO}$ at 630 kHz and equal amplitude are applied to the LO part of the mixers, but the LO signal for mixer 1 is 90° ahead in phase. After that, IF ports of the mixers are connected to the 4$^{th}$ order low pass filter. The signal is converted down to 50 kHz by mixers and the upper sideband signal at 1310 kHz and also harmonics of the mixers are eliminated by LPF. The two signals after the LPFs are both at frequency $IF$ at 50 kHz and of equal amplitude, but the signal behind mixer 2 is 90° ahead in phase. The phase shifter increase the phase difference between two mixer outputs by another 90°, so that the signal at mixer 2 is 180° ahead in phase. After that, the differential amplifier superimposes two signals constructively.

Secondly, the signal from lower sideband at 580 kHz is again applied to both mixers and the properties of the LO signals are exactly same as in the case of upper sideband. In contrast, the output signal behind mixer 1 is 90° ahead in phase. As a result, the phase shifter changes the phase difference between the signal behind mixer 1 and the signal behind mixer 2 to 0°. Therefore, the differential amplifier superimposes two signals destructively. The Trigonometric calculations for both upper sideband signal and lower sideband signal are explained (4.2).

| | Upper Sideband | Lower Sideband |
|---|---|---|
| Input Signal | $\sin((\omega_{LO} + \omega_{IF})t)$ | $\sin((\omega_{LO} - \omega_{IF})t)$ |
| After Mixer Stages<br>Mixer 1<br>Mixer 2 | $\frac{1}{2}((\cos(\omega_{IF})t + 90°) –$<br>$(\cos(2\omega_{IF} + \omega_{IF})t + 90°)),$<br>$\frac{1}{2}((\cos(\omega_{IF})t) –$<br>$(\cos(2\omega_{IF} + \omega_{IF})t))$ | $\frac{1}{2}((\cos(-\omega_{IF})t + 90°) –$<br>$(\cos(2\omega_{LO} - \omega_{IF})t + 90°)),$<br>$\frac{1}{2}((\cos(-\omega_{IF})t) –$<br>$(\cos(2\omega_{LO} - \omega_{IF})t)),$ |
| After LPF | $\frac{1}{2}((\sin(\omega_{IF})t),$<br>$\frac{1}{2}((\cos(\omega_{IF})t)$ | $-\frac{1}{2}((\sin(\omega_{IF})t),$<br>$\frac{1}{2}((\cos(\omega_{IF})t)$ |
| After 90° phase shifter | $\frac{1}{2}((\sin(\omega_{IF})t),$<br>$-\frac{1}{2}((\sin(\omega_{IF})t)$ | $-\frac{1}{2}((\sin(\omega_{IF})t),$<br>$-\frac{1}{2}((\sin(\omega_{IF})t)$ |
| After differential amplifier | $\sin(\omega_{IF})t$ | 0 |

Figure 4.2: Trigonometric calculations for sinusoidal input signals from the upper and the lower sideband to the single sideband down converter

The rejection of the lower sideband leads to improvement in signal to noise ratio in a factor of 2. Therefore, the ultimate goal is to have 3dB improvement in SNR.

## 4.3 Design and Implementation of the SSB Down Converter

Firstly, I designed the PCB board for the SSB down converter and the power splitter using the PCB-CAD software EAGLE. In Figure 5, the schematic and in Figure 6, the layout of the SSB down converter are shown. The SSB down converter consists of 2 mixers, 2 low pass filters, two 90° phase shifters and a differential amplifier. The output of the SSB down converter is connected to a power splitter, in order to use this SSB down converter in feedback cooling. For the SMD mixers, I used TUF-R3SM+ from Minicircuits [22] and for the power splitter, I used SCP-2-1+ from Mini Circuits [23]. These components were selected based on previous experience from the BASE group. The input signal is applied to the RF ports of both mixers. The two local oscillator signals of the mixers have equal frequency $\nu_{LO}$ and equal amplitude, but the local oscillator signal for mixer 1 is 90° ahead in phase. After that, IF ports of the mixers are connected to the 4th order low pass filter (LPF) which was designed using the computer software ELSIE, and in Figure 4.5, the schematic of the LPF and its attenuation graph are shown.

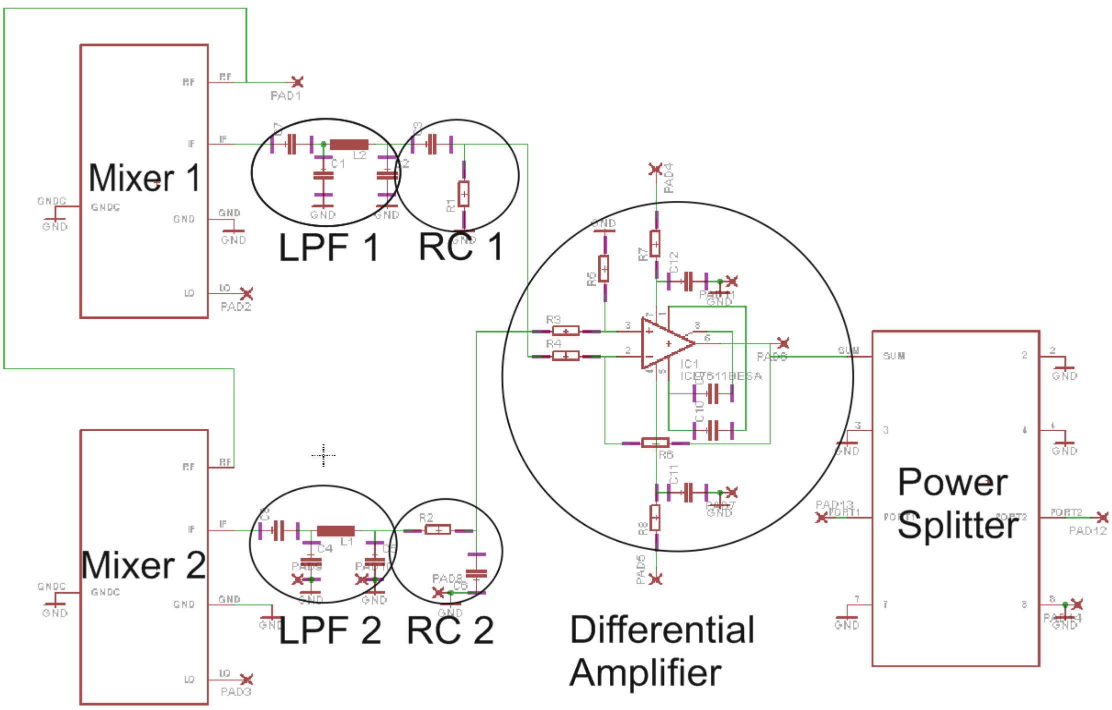


Figure 4.3: Schematic of the SSB down converter consists of 2 mixers, 2 LPFs, 2 RC phase shifters, a differential amplifier, and a power splitter. For further discussion see text.

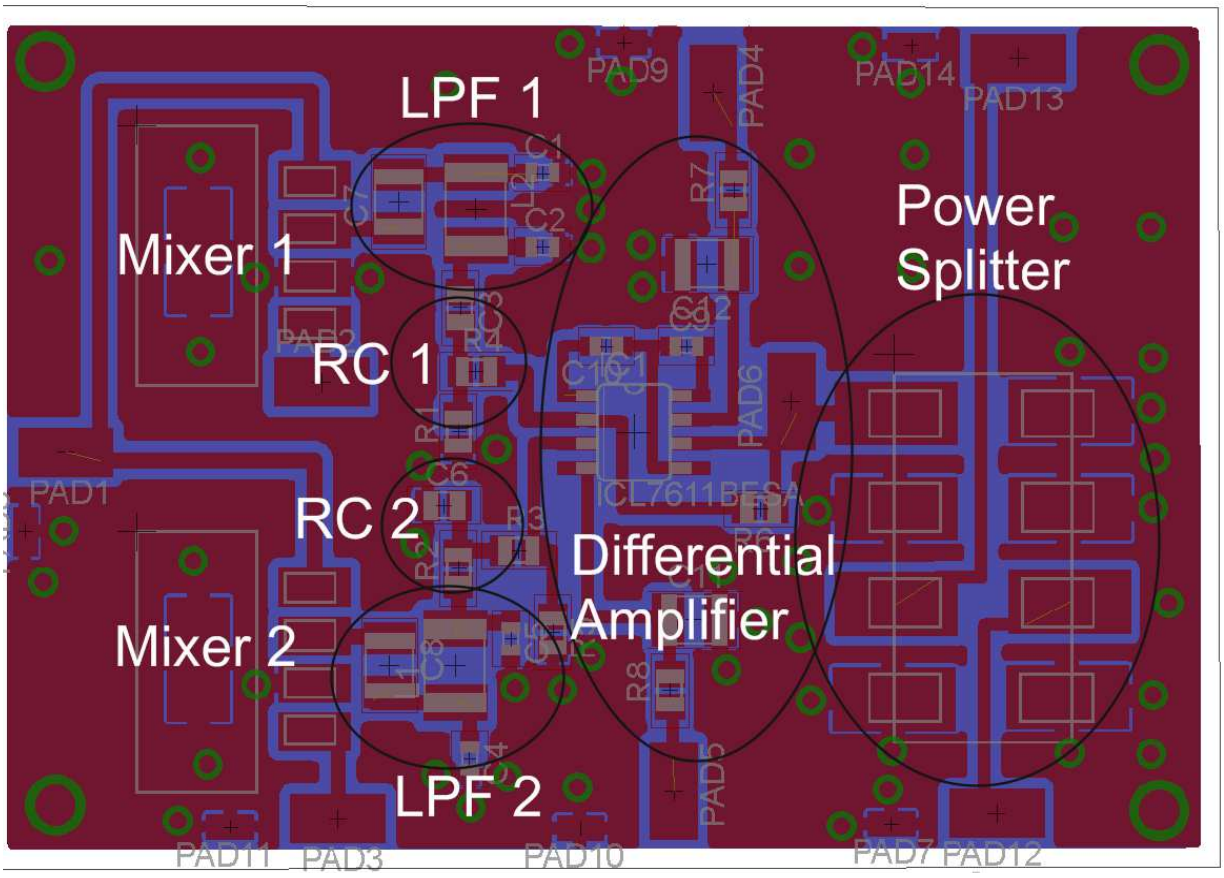


Figure 4.4: PCB layout of the SSB down converter. For details see text.

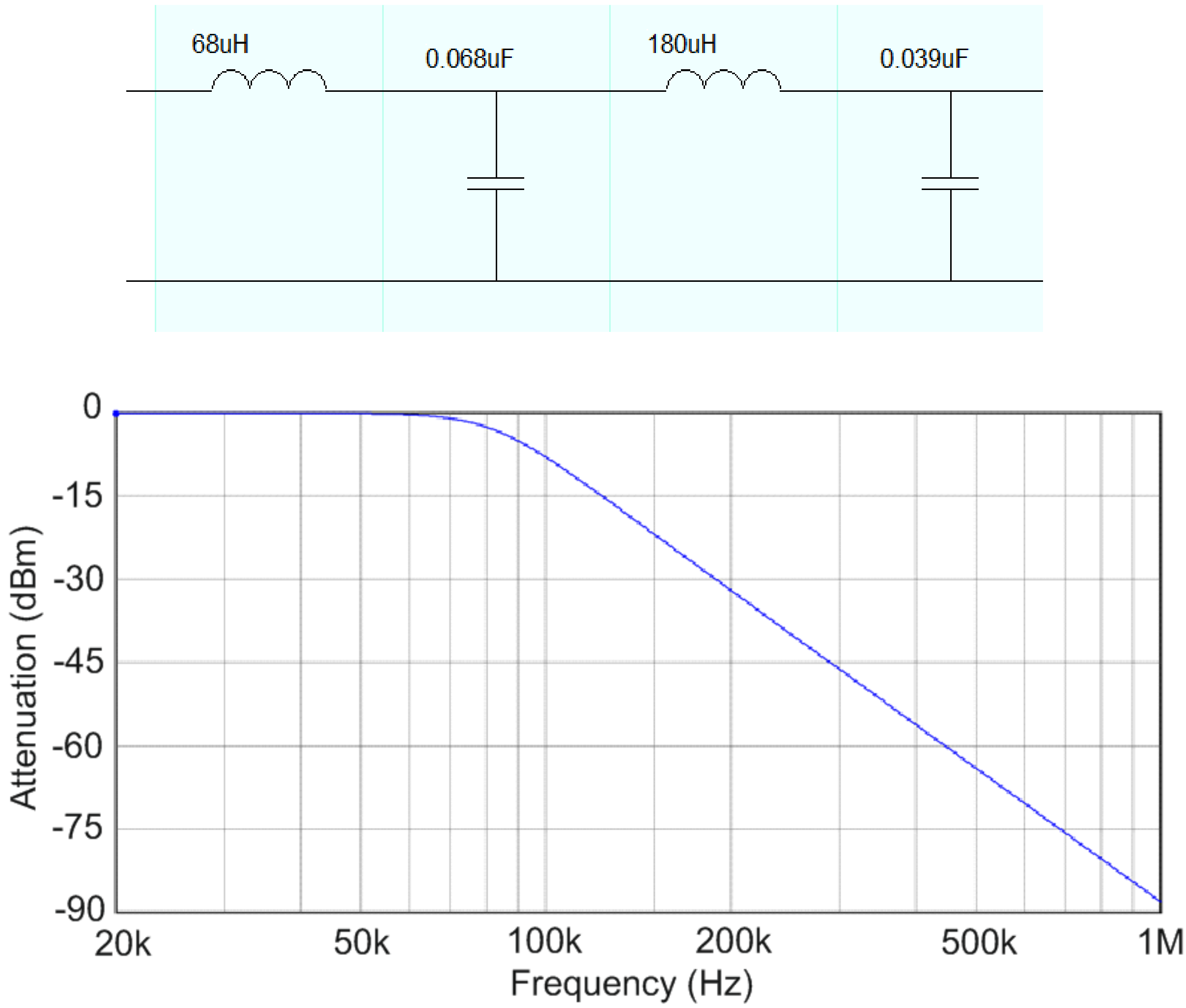


Figure 4.5: Schematic and the attenuation curve of the 4$^{th}$ order LPF. For details see text.

The signal behind the mixer 2 is 90° ahead in phase. Then the second phase shifter increases the phase difference between the signal behind mixer 1 and the signal behind mixer 2 by another 90°, so that the signal behind mixer 2 is 180° ahead in phase. I used a simple RC circuit to change the phase by 90°. I calculated the R and C values by the formula:

$$f_c = \frac{1}{2\pi RC}$$

So, I chose the C value as 220pF and R value as 14.5kΩ. If the phase shifter does not change the frequency exactly 90°, we can tune the phase of the LO signal of mixer 1 to have exactly 180° phase difference before the differential amplifier. At the output of the RC filters, we have two signals with 180° difference in phase. These signals are connected to the differential amplifier. I used a MAX410 low noise op-amp [24], because its noise was very low around 50 kHz. I implemented a differential amplifier by using this op-amp and the output of the amplifier is connected to the power splitter. In Figure 4.6, we can see the PCB of the SSB down converter.

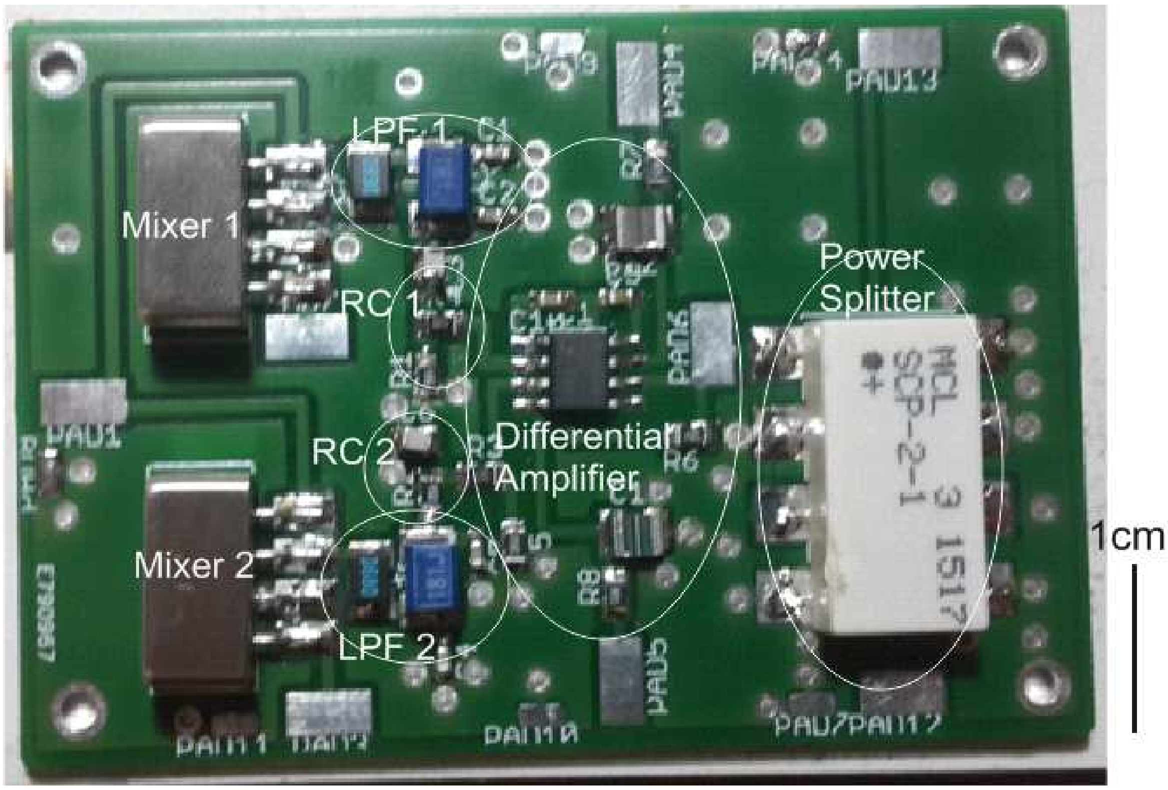


Figure 4.6: PCB of the SSB down converter. For further discussion see text.

### 4.4 Measurement Results of the SSB Down Converter

Firstly, two signal generators, a voltage supply for the biasing of the op-amp and a spectrum analyzer are used for the measurement. A sinusoidal signal at 680 kHz and -56 dBm is applied as an input signal. Two LO signals are applied by the second signal generator which has two output ports. The power of LO signals is +15 dBm and the frequency is at 630 kHz, but the LO signal for mixer 1 is 90° ahead in phase. For biasing voltages of the amplifier, +3V and -3V are applied to the DC biasing ports. As a result, we aim to see an amplified signal at 50 kHz at the output port. In the differential amplifier, we used 150Ω and 150kΩ resistors in order to have 30dB gain at the differential amplifier stage. The loss of the LPF an RC filter stages is about 7dBm, the loss of the power splitter is about 4dBm, and the conversion loss of the mixers is also about 5dBm. As a result, we expect to see 14dB gain in overall system. We applied -56dBm signal at 680 kHz to the input and -46 dBm signal at 50 kHz is observed at the output by the spectrum analyzer. The gain was about 10 dB in measurements, which means we have 4dB additional loss. It is not a crucial problem, because we use ZFL-500LN amplifier before the SSB down converter, and the gain of this low noise amplifier is about 30dB, so we can compensate these losses.

Afterwards, the SSB down converter was connected to the apparatus. The axial motion signal of an antiproton is connected to the input of the SSB down converter via a ZFL-500LN amplifier [25]. Then, one output of the SSB down converter is terminated by 50Ω and the other output is connected to the FFT analyzer. Previously, a discrete ZAD-6+ Minicircuits mixer [26] was used for the down conversion, but it was not a single sideband down conversion process. In Figure 4.7, we can see axial resonance curves with SSB down converter and without SSB down converter. The resonance peak is set to 0dBm and we can calculate SNR by subtracting peak attenuation from background noise level. As can be seen in Figure 4.7, the SNR was about 23 dB in the simple down conversion. By applying SSB down conversion, the SNR is increased to 26dB. Consequently, we achieved 3dB improvement in SNR as expected.

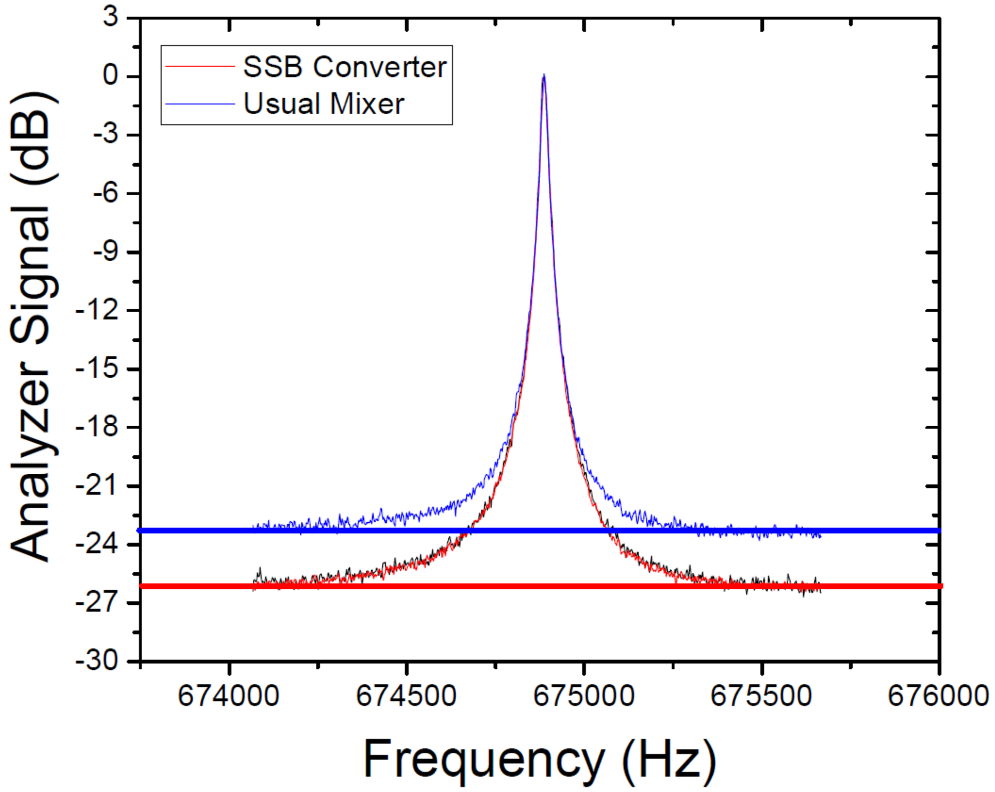


Figure 4.7: Axial resonance curves with SSB down converter and with a simple mixer. To calculate the SNR, attenuation at the peak is subtracted from background level. As a result 3dB SNR improvement is achieved. For further discussion see text.

SNR improvement in axial detection system provides more precise measurements of the axial frequency. So, we expect to see a decrease in axial frequency fluctuation. Axial frequency fluctuations with SSB down converter and without SSB down converter as a function of averaging time are analyzed in Figure 4.8. The axial frequency fluctuation Ξ is proportional to [10]:

$$\Xi \propto \sqrt{\frac{\Delta\nu}{\mathrm{T}}\left(\frac{1}{\sqrt{SNR}}\right)} ,$$

where Δν is the linewidth of the particle dip, T the averaging time of the measurement, and SNR the signal-to-noise ratio of the detector, respectively. If the linewidth is decreased and the SNR is increased, the axial frequency fluctuation will decrease. The frequency fluctuation is characterized by two different noises which are Gaussian white noise, and random walk noise. At small averaging times the Gaussian white noise is dominant, while the random walk noise is dominant in larger averaging times. The axial fluctuation is also reduced by increasing the averaging time, because for long averaging times, Gaussian white noise converges to a lower fluctuation limit [10]. However, random walk noise increases with increasing averaging time, and after a critical point, the random walk noise dominates the axial frequency fluctuation. This effect can be observed in Figure 4.8.

To characterize axial frequency fluctuation, the axial motion signal of an antiproton is connected to a power splitter via a ZFL-500LN amplifier. One output of the power splitter is connected to one channel of the FFT analyzer via the SSB down converter and the second output of the power splitter is connected to second channel of the FFT analyzer via a simple mixer. With this setup we recorded axial frequency data for a total measurement time of 10 hours, and compare the measured axial frequency fluctuation of both channels, for different averaging times, such plots are called Allan deviations. The results are shown in Figure 4.8. Specifically at small averaging times the SSB down converter decreased the axial frequency fluctuation significantly. For instance, at 60s averaging time, the SSB downconverter channel has about 7 mHz improved axial frequency fluctuation. The frequency fluctuation comes from Gaussian white noise is proportional to [10]:

$$\Xi \propto \sqrt{(\frac{\mathrm{Ndef}}{\sqrt{T}})^2 + (\frac{\mathrm{Nlsb}}{\sqrt{T}})^2}\ .$$

$N_{lsb}$ is the noise constant comes from lower sideband signal. By applying SSB down conversion, this noise constant will be rejected and this decreases the axial frequency fluctuation. However, axial frequency fluctuation becomes equal with and without SSB down converter at high averaging times, because after a particular averaging time, random walk noise becomes dominant and the frequency fluctuation is solely defined by the walk [2,10].

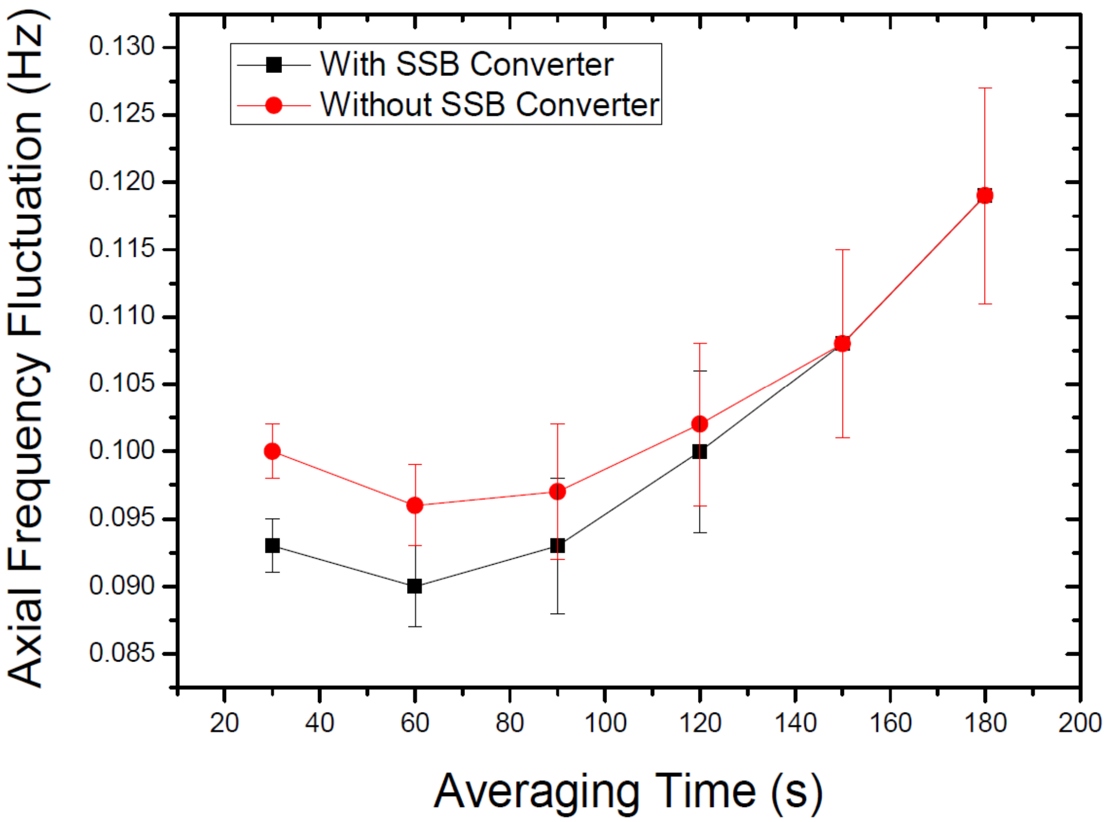


Figure 4.8: Axial Frequency Fluctuation wrt. averaging time with and without SSB down converter

This increases the fidelity of the spin flip detection. To identify the spin-state, we apply the threshold method, assuming that every frequency change above a certain limit is a spin-flip [2]. Fidelity is the probability of that the identification of the spin state at a given threshold is correct. In an ideal measurement, if we assume the axial frequency fluctuation is 0 mHz, the fidelity is 100%. We could observe a difference of S = 50% spin flip probability between resonantly driven spin-flips and off resonantly driven spin flips [10]. It is the theoretical limit. As we see in Figure 4.8, the axial jitter is at least 90 mHz in our detection system. The SSB down converter decreases the axial jitter, consequently it will also increase the fidelity. Figure 4.9 shows us the fidelity with and without SSB down converter. The maximum value of the fidelity is 72.3% without SSB down converter and 74.5% with SSB down converter. There is 2.2% increase in the fidelity for spin flip detection. In case of a Fidelity F lower than 100%, we can calculate the signal intensity *S* given as the difference of observed spin-flips with the threshold method for resonantly and off-resonantly driven spin flips [10]:

$$S = 0.5 - (1 - F),$$

As a result, without SSB down converter, *S* is 22.29% which is at the edge of being able to perform measurement, and *S* becomes 24.52% with SSB down converter. So, the gain in signal strength can be calculated;

$$\frac{0.2452}{0.2229} = 1.10$$

With the SSB down converter, we gain relative 10% in the signal strength, which reduces the total measurement time required to resolve the magnetic moment significantly.

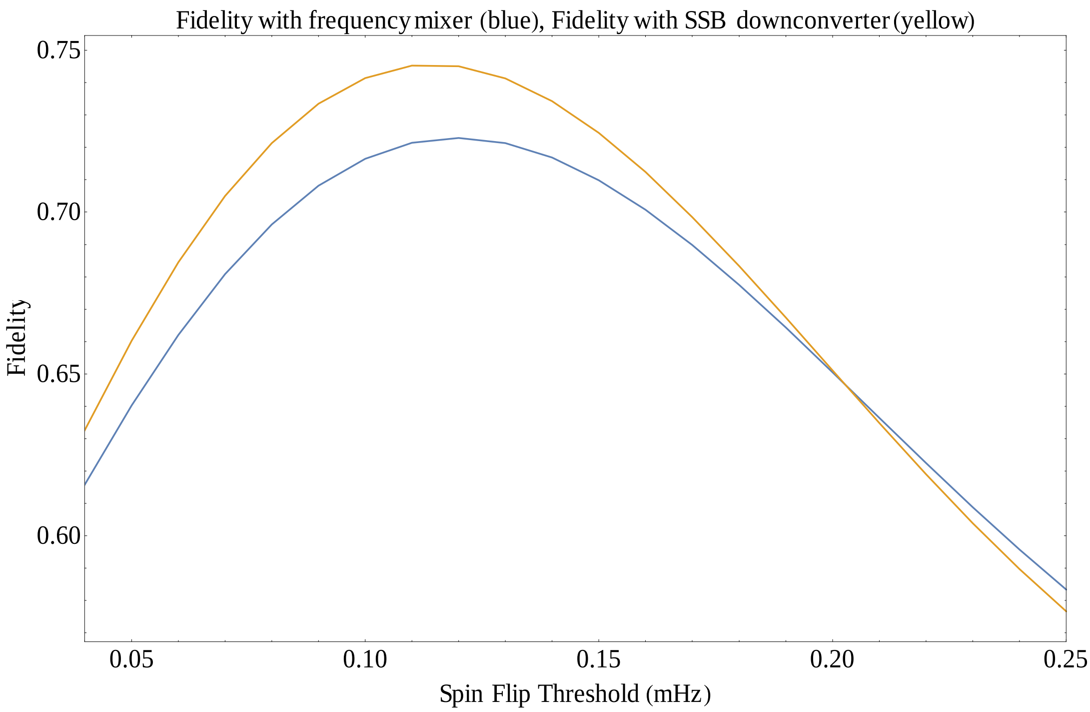


Figure 4.9: Fidelity with and without SSB down converter

# Chapter 5

# Active Feedback Cooling

### 5.1 Theoretical Concepts of Active Feedback Cooling

In order to resolve tiny axial frequency changes for spin flip detection, we need to have a good resolution on the axial frequency. Since the axial frequency resolution depends on the dip width ($\Delta\nu$), and $\Delta\nu$ is proportional to the Q value of the axial detector, a decrease of the Q-value will lead to a decrease of the linewidth of the dip and thus increase frequency resolution. Such a tuning of the linewidth can be achieved by application of active electronic feedback cooling. In addition, application of active feedback reduces the particle temperature which leads to a variety of benefits, as lower drive power, reduced line width, and faster particle preparation cycles. Overall, application of feedback cooling will speed up experiment routines and eventually lead to measurements at improved precision. A detailed discussion of all the involved effects is beyond the scope of this thesis, for an exhaustive discussion see [7,10].

The measured power spectrum has a constant baseline due to the Johnson noise. The current induced by the noise-driven protons or antiprotons produces a notch in this flat spectrum at axial frequency $\nu_z$. The angular frequency width of this notch is the damping rate $\Gamma$. The relationship between the damping rate, effective temperature and the feedback gain is given as [7]:

$$\Gamma_e = (1-g)\Gamma$$

$$T_e = (1-g)T,$$

or in other words: The ratio $\Gamma_e / T_e$ is a fluctuation/dissipation invariant. The temperature decreases as the feedback gain is increased. Noiseless feedback gain $0 < g < 1$ decreases temperature, but at the expense of reducing the damping rate. The advantage of a reduced $T_e$ is to reduce deleterious effects of axial fluctuations upon other particle motions, as we will illustrate with a reduced linewidth. According to literature [7] it is possible to decrease the effective temperature in a factor of 5 by using active feedback cooling.

### 5.2 Working Principles of Active Feedback Cooling

In Figure 5.1 a schematic of the devices used for active feedback cooling system is shown. Without the feedback cooling system, the LNA at 300 Kelvin stage is connected to the FFT analyzer via a down converting mixer. In the active feedback cooling, the output of the LNA is connected to the SSB down converter. After that, the signal from SSB down converter goes to a power splitter. Half power of the signal is connected to the FFT analyzer to observe the resonator spectrum, the other half is connected to the axial detector via an up converter, a band pass filter and a voltage controlled attenuator (VCA). The output of the VCA is connected to the detection system lose capacitive coupling.

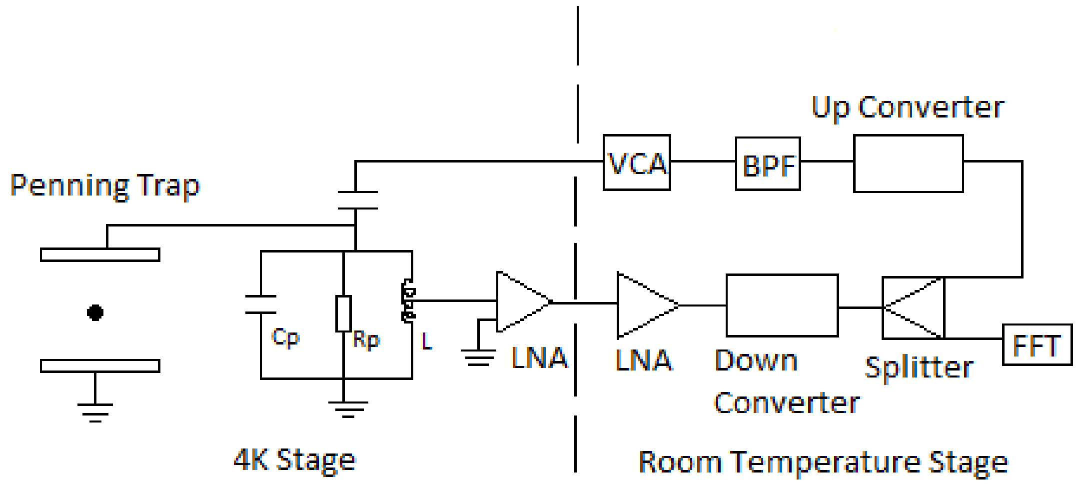


Figure 5.1: Schematic of active feedback cooling system consists of an SSB down converter, a power splitter, an up converter, a BPF and a VCA. For further discussions see the text.

The temperature of the axial detection system is around 8 Kelvin. By using active feedback cooling, we intend to decrease this temperature approximately by a factor of 3 to 5.

### 5.3 Design and Implementation of the Active Feedback Cooling

The active feedback cooling system consists of a SSB down converter, a power splitter, an up converter, a bandpass filter and a voltage controlled attenuator. After these separate parts are developed, these boards are connected to each other as shown in Figure 5.1. Development of the SSB down converter and power splitter has been explained in section 3.3. In this part, the development of the BPF, the Up-Converter and the VCA will be explained.

#### 5.3.1 Band Pass Filter

A band pass filter (BPF) is a device which passes frequencies within a certain range and rejects frequencies outside that range. For the band pass filters, the two basic resonant strategies are these: series LC to pass a signal or parallel LC to short a signal. By increasing the number of LC stages, we can have sharper attenuation curve, but the resonant frequencies of all LC stages should be equal to have minimal attenuation at the passband.

At first, we intended to develop a $5^{th}$ order BPF, however the attenuation in the passband was high about 10dBm, because it is very hard to have exactly same resonant frequencies in all LC stages. Therefore, I developed a $3^{rd}$ order BPF.

I set the central frequency to 674850Hz, which is the axial frequency. In Figure 5.2, we can see the schematic and the attenuation curve of the $3^{rd}$ order BPF. The attenuation curve is not very sharp as in $5^{th}$ order BPF, however measurement results are very well for our case. As we can see in Figure 5.3, the attenuation in the passband is only 1.9dBm and the attenuation difference between the axial frequency $\sim$ 675 kHz and the cyclotron frequency $\sim$ 18.7 MHz is about 80dBm. Furthermore, the measured attenuation characteristic of the $3^{rd}$ order BPF is 50dB/decade which is enough for our case.

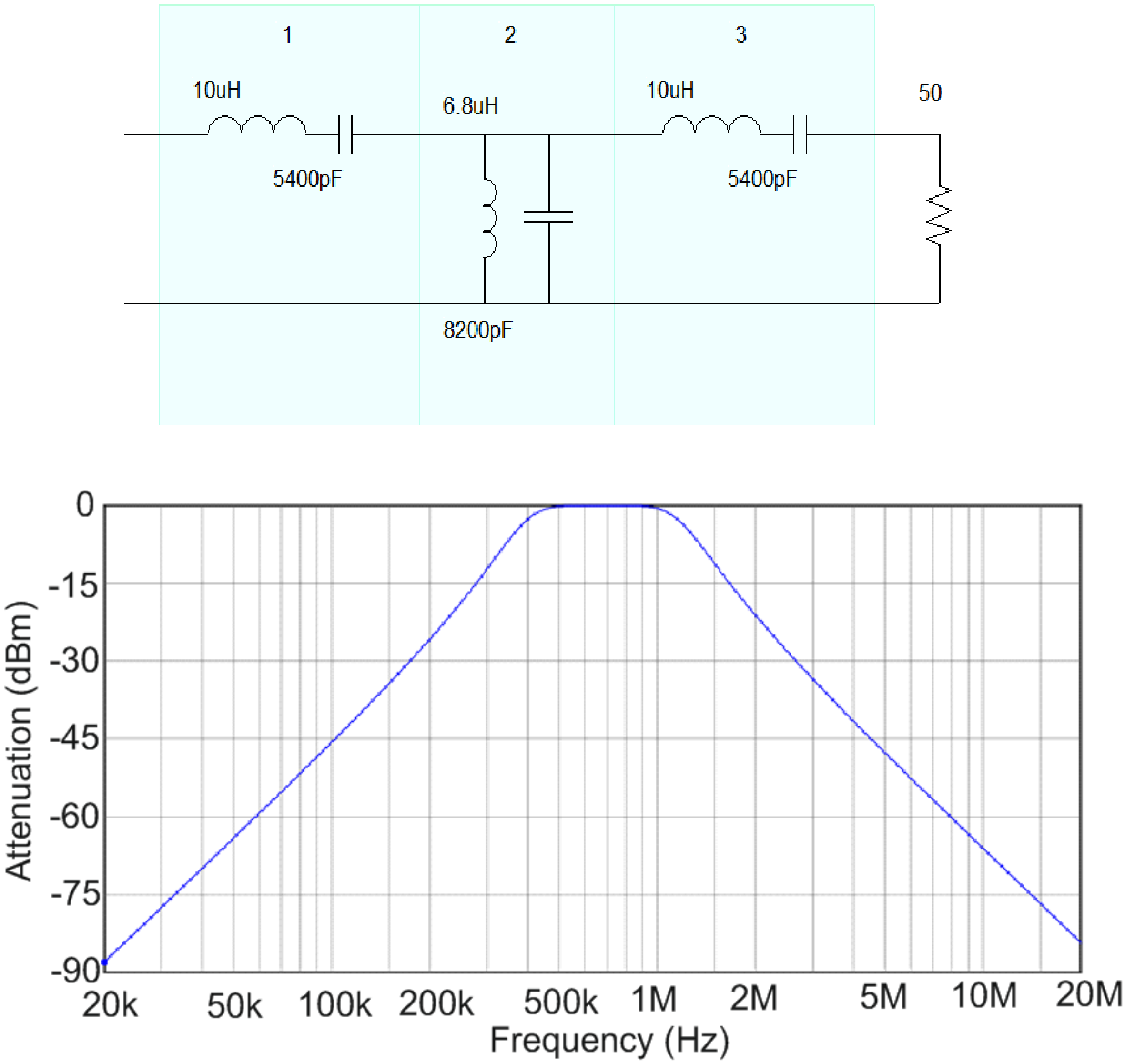


Figure 5.2: Schematic and the simulated attenuation curve of the 3rd order BPF

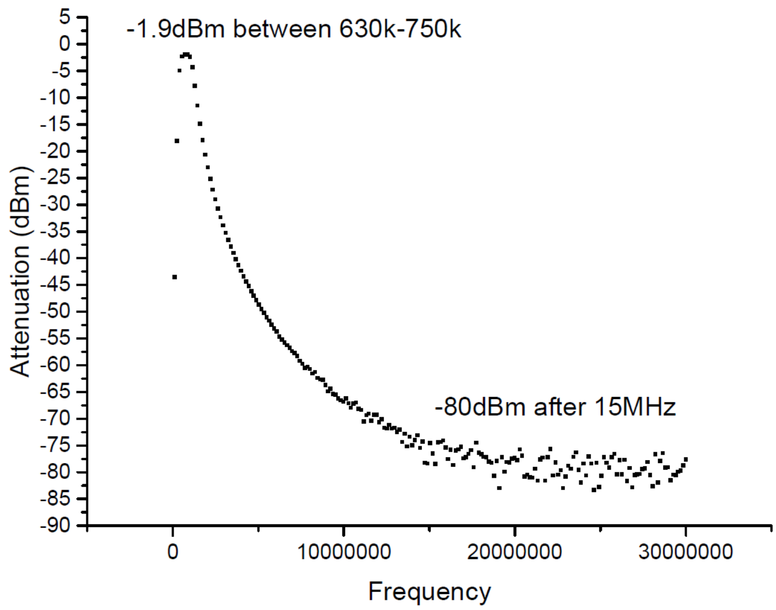


Figure 5.3: Measured attenuation curve of the 3rd order BPF

### 5.3.2 Voltage Controlled Attenuator

I designed and implemented the voltage controlled attenuator for the feedback cooling system. We intended to have 20dB attenuation range. In Figure 5.4, the schematic and the layout of the VCA are shown.

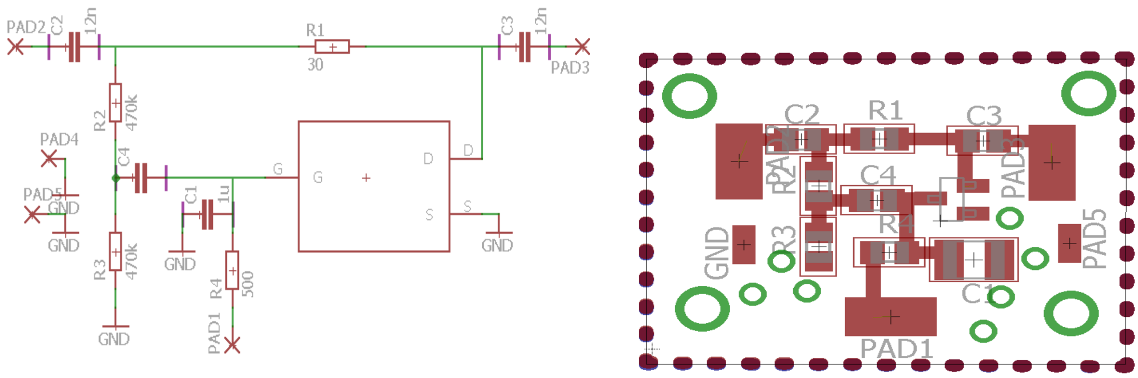


Figure 5.4: Schematic and PCB layout of the VCA. The transistor is used as a voltage variable resistor, and the attenuation is controlled by tuning its gate-to-source voltage.

In this VCA, BF862 N channel JFET [27] transistor is used as a voltage variable resistor. By changing the gate to source voltage of the JFET, we can control the attenuation of the system. In Figure 5.5, the PCB and the measured attenuation as a function of the biasing voltage is shown

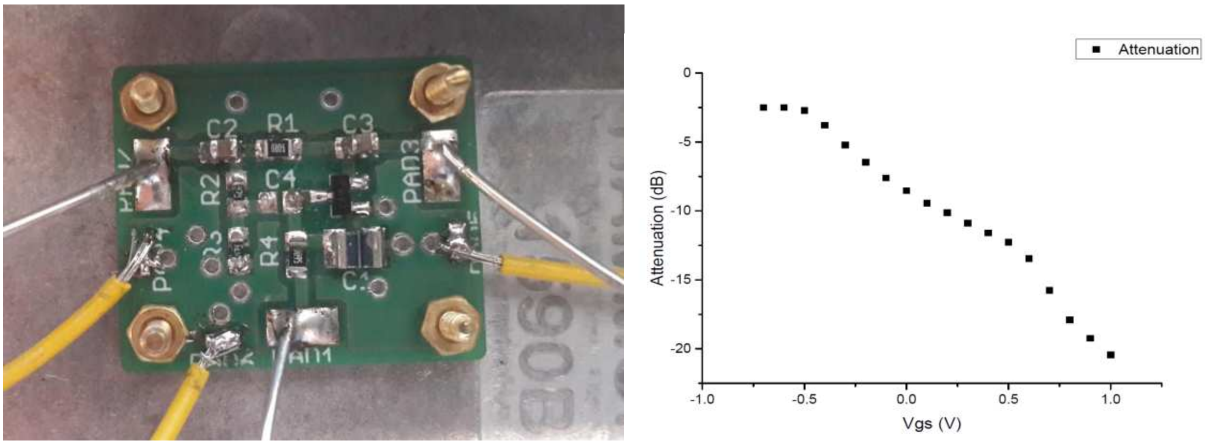


Figure 5.5: PCB and Attenuation wrt. $V_{gs}$ Graph of the VCA

As we see, the attenuation range is around 20dB as intended. When $V_{gs}$ is around 1 V, the drain to source resistance of the JFET is very low around 5 to 10 ohms. When we decrease the $V_{gs}$, the drain to source resistance ($R_{ds}$) starts to increase and we can use the JFET as a voltage variable resistor. The gain can be calculated as follows;

$$g = \frac{Rds}{Rds + R1}$$

So, by changing the biasing voltage, we can modify the attenuation. For maximum attenuation, we apply +1V and for minimum attenuation, we apply -0.7V.

### 5.3.3 Up Converter

For the up conversion part, we only used a single mixer. We used TUF-R3SM+ SMD mixer [22] as we used also in down conversion part. A signal with a power of +15dBm and with a frequency of 630kHz is applied to the LO input of the mixer. The RF input of the mixer is connected to one output of the SSB down converter and the IF output of the mixer is connected to the BPF.

### 5.4 Test of the Axial Detector with and without Active Feedback Cooling

After completion of the individual parts, we tested the active feedback cooling in the BASE apparatus. The input of the SSB down converter was connected to the output of a ZFL-500LN ultra-low noise amplifier [25]. One output of the SSB down converter is connected to the FFT analyzer and the other output is connected to the input of the up converted to apply a feedback. The output of the up converter is connected to the input of the VCA via the axial BPF and the output of the VCA is connected to the detection system via sub-pF capacitance.

Figure 5.6 shows the active feedback cooling system attached to the apparatus. We applied positive and negative feedback and checked the axial resonance signal. The temperature change can be calculated by using below formulas [10]:

$T_{eff} = T_0\,(1 \pm G_{FB})$

$R_{eff} = R_p\,(1 \pm G_{FB})$

$R_{eff} = \omega_0 L \mathrm{Q}$

$\mathrm{Q} = \omega/\Delta\omega$

Q is the Q-factor of the axial detector, $\omega_0$ is the central frequency of the axial resonator, $L$ is the inductance value of the axial resonator and $R_{eff}$ is the effective resistance seen by the particle if feedback is applied, and $R_p$ is the resistance without feedback. $T_0$ is the temperature of the axial detector without feedback, and $T_{eff}$ is effective temperature if feedback is applied [10,15].


Figure 5.6: Active feedback cooling system attached to the apparatus

We can see the axial resonance graph with positive feedback in Figure 5.7. Figure 5.8 shows the Q-factor of the resonator and the effective temperature of the detector with respect to Vgs of the VCA. We set the gain-to-source voltage of the transistor in the VCA from 0 V to 1 V. By decreasing the biasing voltage, we increase the gain of the feedback. It results in an increase in the Q-factor and effective temperature. The temperature of the detector was about 8 K without feedback, and if we apply full positive feedback signal, the temperature increases by 50 to 60 K. We have to apply negative feedback to decrease the temperature. Figure 5.9 shows axial resonance graph with negative feedback. We set the Vgs of the transistor in the VCA from -1 V to +1 V. As shown in Figure 5.10, the gain of the feedback is increased by reducing the Vgs, and it leads to a reduction in the Q-factor of the resonator and the effective temperature of the detector. When we set the biasing voltage of the VCA to -0.7 V, the gain becomes maximum about 2/3, and $T_{eff}/T_0$ becomes equal to 0.3473. It means that we can decrease the temperature in a factor of 3 by using this negative feedback cooling. The temperature of the axial detector was 8 Kelvin without feedback cooling, and we can decrease it to 2.6 Kelvin by connecting the negative feedback cooling.

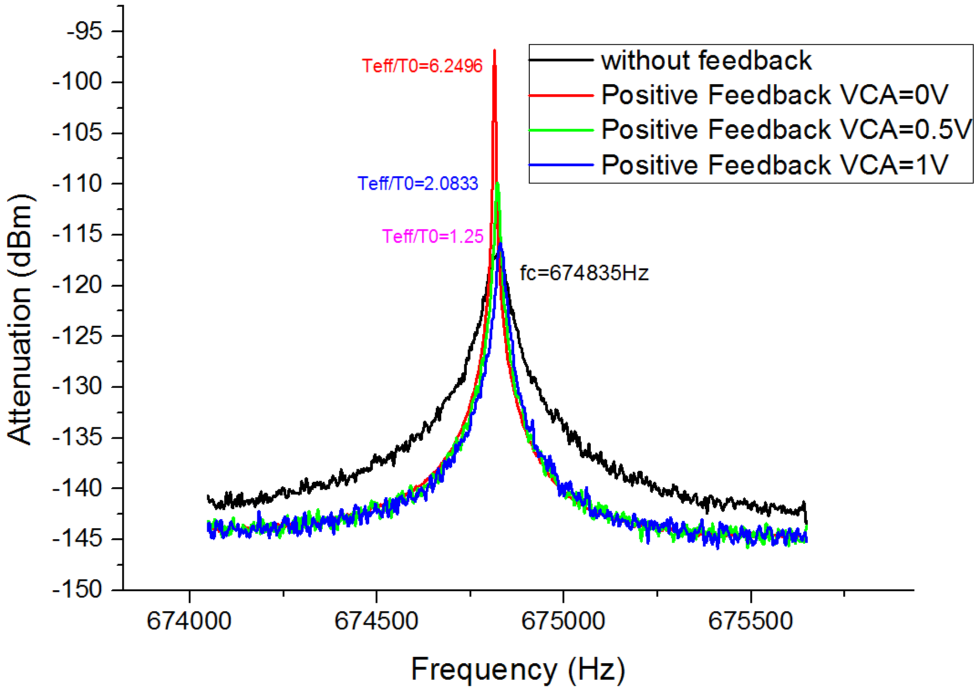


Figure 5.7: Axial resonance frequency with positive feedback. Effective temperature increases with positive feedback. For further discussion see text.

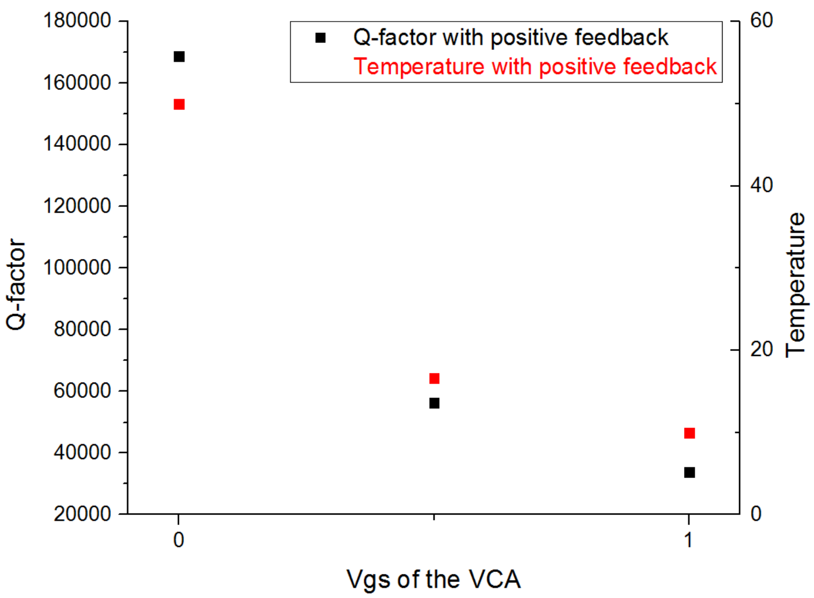


Figure 5.8: Q-factor and effective temperature of the detector with positive feedback. If the biasing voltage of the VCA is decreased, it increases the gain of the feedback and results in a rise in the Q-factor and the effective temperature of the detector.

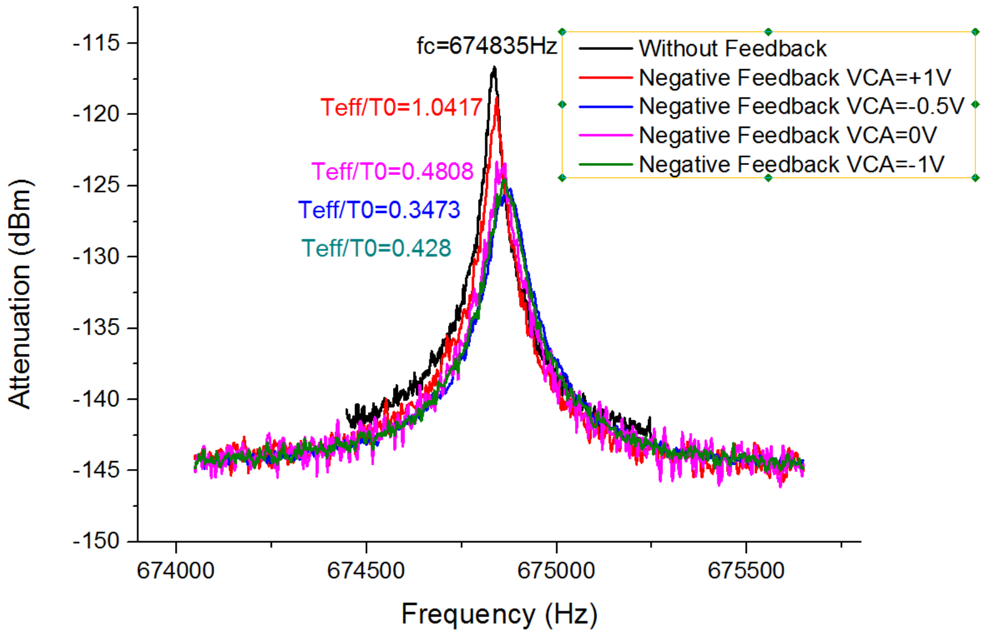


Figure 5.9: Axial resonance frequency with negative feedback. Effective temperature decreases with negative feedback. For further discussion see text.

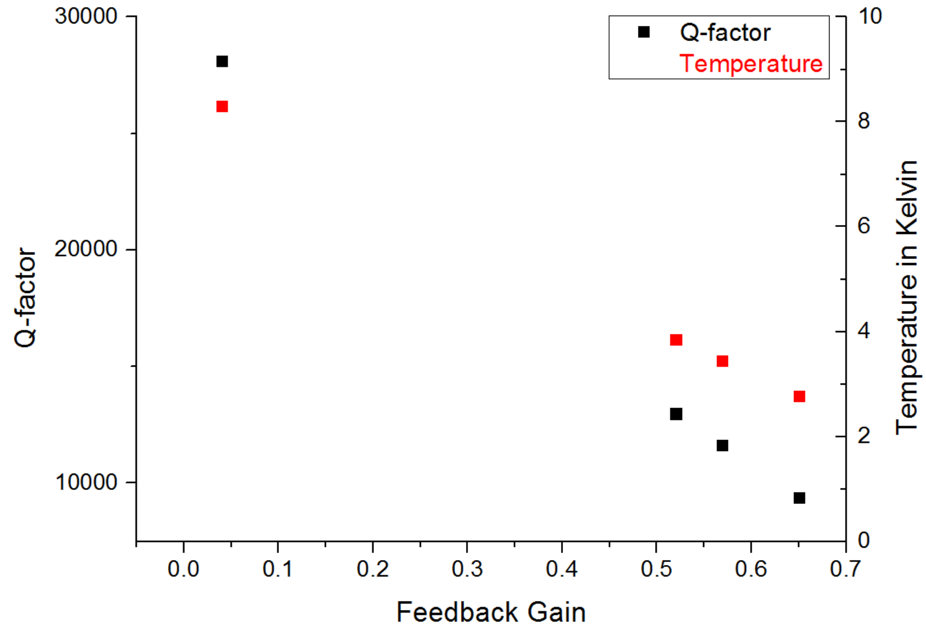


Figure 5.10: Q-factor and effective temperature of the detector as a function of negative feedback gain. If the biasing voltage of the VCA is decreased, it increases the gain of the feedback and results in a reduction in the Q-factor and the effective temperature of the detector.

After that, we transported an antiproton to analysis trap and checked the line width of the particle with and without feedback cooling. For feedback cooling, we set the biasing voltage of VCA to -0.5V we applied negative feedback. The axial dip with and without feedback is given in Figure

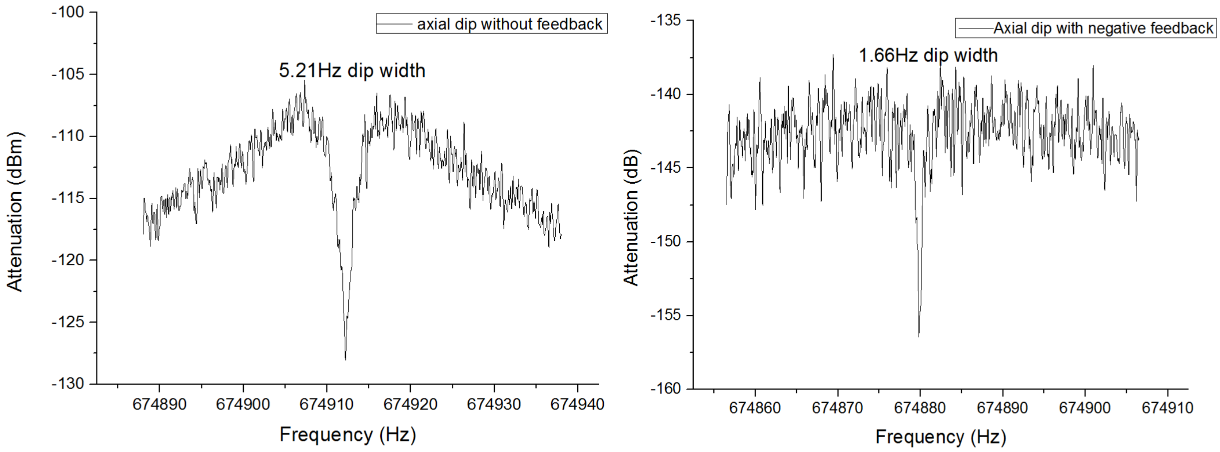


Figure 5.11: Axial dip without feedback (left) and with feedback (right). Negative feedback reduces the linewidth of the dip from 5.21Hz to 1.66Hz. For details see text.

We measured the linewidth without negative feedback for 412 different axial data, and the linewidth with feedback for 23 different axial data. The histogram of the linewidth measurements are shown in Figure 5.12. We calculated the mean and standard deviation of both data set. We can say that these data points are scattered almost in Gaussian distribution. The mean of the linewidth is about 5.215 without feedback cooling and 1.666 with active feedback cooling. As a consequence, the linewidth of the axial detection system is reduced in a factor of 3.13.

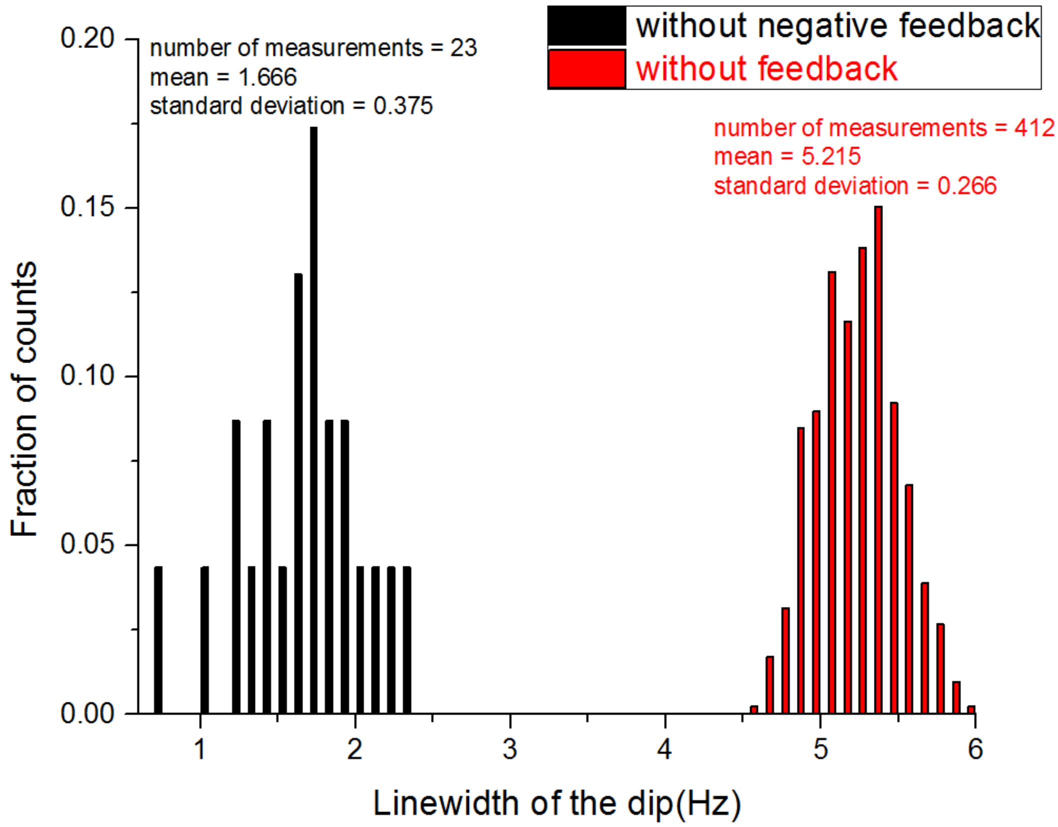


Figure 5.12: Histogram of the linewidth of the axial dip without feedback (right) and with feedback (left). Axial dip is reduced in a factor of 3.13 by applying negative feedback.

# Chapter 6

# Cryogenic Filters for the Spin-flip lines

### 6.1 Motivation

To drive spin transitions, strong radio-frequency drives with powers up to 30dBm are needed. Such high power drives produce spurious noise and heats the radial eigen-motions such as the modified cyclotron mode and the magnetron mode [2]. The fluctuations couple via a magnetic inhomogeneity to the axial frequency and axial frequency stability is reduced, which makes the detection of spin transitions challenging. Therefore, I developed and characterized cryogenic filters for the spin-flip lines, to suppress spurious heating of the radial modes in the analysis trap (AT).

### 6.2 Design and Implementation of the Filters

These filters will be used in the superconducting BASE magnet under high magnetic field and at 4 Kelvin. Therefore, the capacitors and inductors should be selected in such a way that they work reliably at cryogenic temperatures and under high magnetic field. For instance, the components should not be ferrite core, because they are strongly affected under high magnetic field. I selected Panasonic ECHU series capacitors, and their dielectric type polyphenylene sulphide (PPS). Therefore, it is not affected under high magnetic field and also it works well at 4K. I selected Johanson technology inductors which are wirewound on ceramic core. Figure 6.1 shows the schematic of the filter. This cryogenic filter consists of two different parts that are 3$^{rd}$ order notch filter and 1$^{st}$ high pass filter (HPF). We aim to reject cyclotron frequency in the AT $\sim$ 18.7 MHz and magnetron frequency $\sim$ 12 kHz. Furthermore, we want to have low attenuation at axial frequency $\sim$ 680 kHz and at Larmor frequency $\sim$ 52 MHz. The central frequency of the notch filter is set to 18.7 MHz in order to reject the modified cyclotron frequency in the analysis trap. A 1$^{st}$ order HPF is applied in order to reject magnetron frequency. At first, we have applied 3$^{rd}$ order HPF in order to have full signal at axial frequency and to have very low attenuation at magnetron frequency. However, this HPF involved a high inductor about 12uH and such high inductances are strongly affected under high magnetic field. Therefore, I used a 1st HPF which consists of a single capacitor.

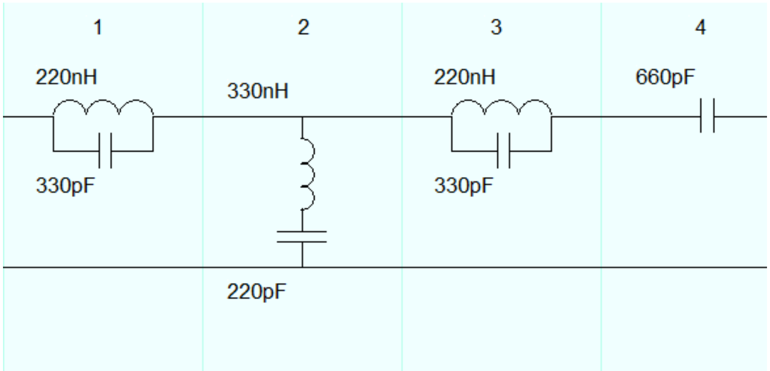


Figure 6.1: Schematic of the cryogenic filter for spin-flip drives. It consists of a 3rd order notch filter and a 1st order HPF. For further discussion see text.

### 6.3 Test of the Filters and Measurement Results

At first, these filters are tested at room temperature. After that, I used a pulse tube cryo-cooler for cryogenic test measurements. Figure 6.2 shows the attenuation curve of the filter at room temperature and also at 4 Kelvin. As can be seen, there is almost no difference between 300K and 4K characteristics. I used a neodymium-alloy permanent magnet with a near-field of 0.8T in order to test the filter under high magnetic field. We found that the filter is not affected under high magnetic field. As we can see in Figure 6.2, we have high attenuation at 12 kHz and at 18.7 MHz and low attenuation at 680 kHz and 52 MHz.  These filters will be implemented in the next run of the BASE experiment. It is expected that the implementation of these filters will improve the axial frequency stability.

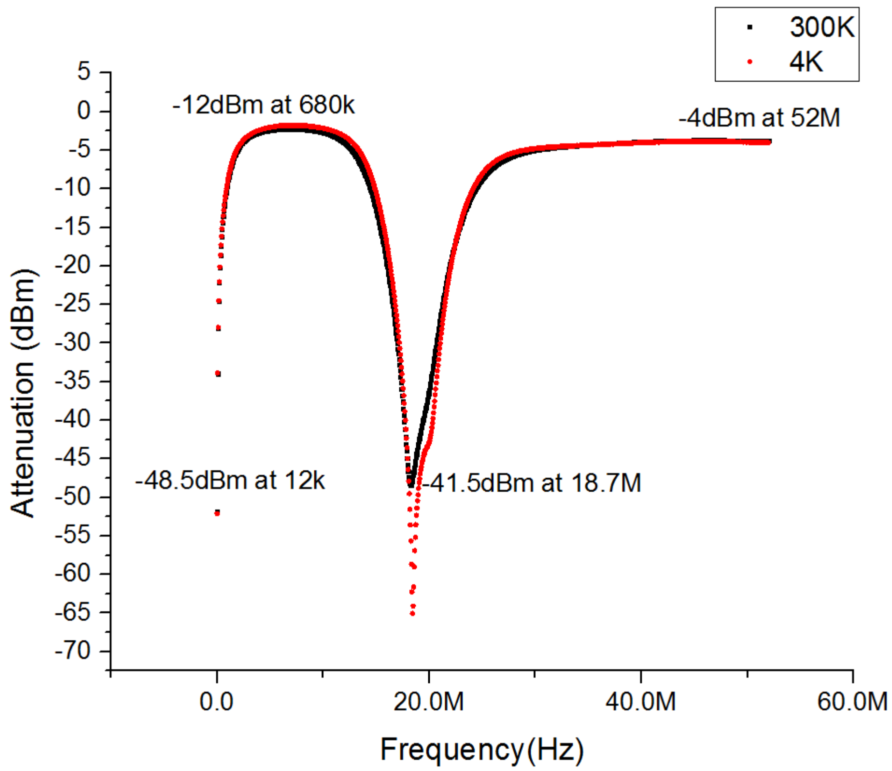


Figure 6.2: Attenuation characteristics of the filter at 300K and at 4K. For details see text.

# Chapter 7

# Conclusion and Outlook

During my time in the BASE Collaboration at CERN, I developed single sideband (SSB) down converter and active feedback cooling for precise measurements of the axial frequency of a single trapped antiproton. I also developed cryogenic filters for the spin-flip lines.

Firstly, I designed and implemented an SSB down converter and then I tested it. As a result, we achieved 3 dB improvement in SNR of the axial detector, 7 mHz improvement in the axial frequency fluctuation at small averaging times. Furthermore, the fidelity is increased and we gain relative 10% in the signal strength, which reduces the total measurement time required to resolve the magnetic moment significantly.

Secondly, I developed an active feedback cooling system. For this part, an SSB down converter, a band-pass filter, an up converter and a voltage controlled attenuator are designed and implemented. After that, I characterized these parts separately and then tested the feedback loop. As a consequence, the temperature of the axial detector is decreased in a factor of 3 from 8 Kelvin to 2.6 Kelvin. Furthermore, the linewidth of the dip is reduced in a factor of 3.1 from 5.21 Hz to 1.66 Hz.

Lastly, I designed and implemented cryogenic filters for the spin-flip lines, which will be implemented in the BASE superconducting magnet. I tested these filters at 4 Kelvin and also under high magnetic field. These works well at cryogenic conditions and also under high magnetic field, and we can reject cyclotron frequency and magnetron frequency spectrum.

For further improvements, we can adjust the gain of the feedback line in a more sensitive way by tuning the gate-to-source voltage of the transistor sensitively. Maybe we can decrease the temperature until 1.8 Kelvin. Cryogenic filters for the spin-flip lines will be used next antiproton-beam time and we expect to decrease the noise which comes from high spin-flip drives.

With these projects, I gained plenty of experience in ultra-low noise electronics. I got used to use several measurement devices such as FFT analyzer, network analyzer and spectrum analyzer. I have also studied in cryogenics and superconducting materials. With this project, I used to work in a high precision experiment. In my opinion, this project was a crucial step in my future academic plans.

I would like to thank Yasar Gurbuz, my professor and supervisor at Sabanci University, and Stefan Ulmer, the team leader of the BASE Collaboration at CERN and my supervisor, and also my colleagues in BASE Collaboration for their continuous supports for my project.

# Bibliography


1. Dörr, S. Setup, test and optimization of detection electronics for high-precision mass measurements at PENTATRAP (2011).

2. C. Smorra, K. Blaum, L.Bojtar, M. Borchert, K.A. Franke, T. Higuchi, S. Sellner, T. Tanaka, S. Ulmer, Eur. Phys. J. Special Topics 224, 3055-3108 (2015).

3. Ulmer S, Mooser A, Blaum. K, Franke K, Kracke H, Leiteritz C, et al.. The Magnetic Moments of the Proton and the Antiproton. J. Phys. Conf. Ser. 2014;488:012033. (2014).

4. Ulmer S, Smorra C, Mooser A, Franke K, Nagahama H, Schneider G, et al.. High-precision comparison of the antiproton-to-proton charge-to-mass ratio. Nature. 2015;524:196–199. (2015).

5. R.S. Van Dyck, et al., Phys. Rev. Lett. 59, 26 (1987).

6. H. Dehmelt, P. Ekstr¨om, Bull. Am. Phys. Soc. 18, 72 (1973).

7. B. D’Urso, B. Odom, G. Gabrielse, Feedback Cooling of a One Electron Oscillator, (2003).

8. J. R. Pierce Theory and Design of Electron Beams, D. van Nostrand Co., NewYork (1949).

9. L. S. Brown and G. Gabrielse, Rev. Mod. Phys. **58**, 233 (1986).

10. S. Ulmer, Ph.D thesis, University of Heidelberg, Germany (2011).

11. Higuchi, T. Master Thesis, University of Tokyo, Japan (2015).

12. S. Ulmer, H. Kracke, K. Blaum, S. Kreim, A. Mooser, W. Quint, C. C. Rodegheri, and J. Walz, Rev. Sci. Inst. 123302 (2009).

13. J. Johnson, Phys. Rev. **32**, 97 (1928).

14. H. Nyquist, Phys. Rev. **32**, 110 (1928).

15. Nagahama, H. Master Thesis, University of Tokyo, Japan (2014).

16. BASE technical design report submitted to CERN, http://cds.cern.ch/record/1503514?ln=ja.

17. Smorra C, Blaum K, Franke K, Matsuda Y, Mooser A, Nagahama H, et al. Towards a high-precision measurement of the antiproton magnetic moment (2014).

18. Mooser A, Ulmer S, Blaum K, Franke K, Kracke H, Leiteritz C, et al.. Direct High-Precision Measurement of the Magnetic Moment of the Proton. Nature. 2014;506:596. (2014).

19. Smorra C, Mooser A, Franke K, Nagahama H, Schneider G, Higuchi T, et al.. A reservoir Trap for Antiprotons. International Journal of Mass Spectrometry. 2015;389:10 - 13. (2015).

20. L. S. Brown and G. Gabrielse, Phys. Rev. A. 2423 (1982).

21. S. Ulmer, C. C. Rodegheri, K. Blaum, H. Kracke, A. Mooser, W. Quint, and J. Walz, Phys. Rev. Lett. 253001 (2011).

22. TUF-R3SM+ mixer datasheet,

https://www.minicircuits.com/pdfs/TUF-R3SM+.pdf

23. SCP-2-1+ power splitter datasheet,

https://www.minicircuits.com/pdfs/SCP-2-1.pdf

24. MAX410 op-amp datasheet,

https://datasheets.maximintegrated.com/en/ds/MAX410-MAX414.pdf

25. ZFL-500LN low noise amplifier datasheet,

https://www.minicircuits.com/pdfs/ZFL-500LN+.pdf

26. ZAD-6+ mixer datasheet,

http://194.75.38.69/pdfs/ZAD-6.pdf

27. BF862 N-channel JFET

http://www.nxp.com/documents/data_sheet/BF862.pdf

28. Panasonic ECHU series capacitors,

https://industrial.panasonic.com/cdbs/www-data/pdf/RDI0000/ABD0000C1.pdf

29. Johanson Technology wirewound on ceramic core inductors,

http://www.johansontechnology.com/downloads/jti-cat-ww-ind.pdf